

## Amorphous-crystalline boundary dynamics in cw laser crystallization

H. J. Zeiger, John C. C. Fan, B. J. Palm, R. L. Chapman, and R. P. Gale  
*Lincoln Laboratory, Massachusetts Institute of Technology, Lexington, Massachusetts 02173*

(Received 5 October 1981)

Two theoretical descriptions have been developed for the phase-boundary dynamics during crystallization of amorphous films by scanning with the slit image of a cw energy beam. The first reduces the problem to the solution of a one-dimensional integral equation, which allows a choice of initial conditions. Depending on the background temperature, numerical solutions yield either periodic or runaway motion of the amorphous-crystalline (*a-c*) boundary, as observed in experiments on scanned laser crystallization of thin films of *a-Ge* on fused-silica substrates. The calculations give a semiquantitative fit to the experimental results for the spatial periodicity observed in the crystallized films as a function of background temperature. Profiles of film temperature as a function of distance from the laser image at successive times have been computed for both the periodic and runaway cases. The model qualitatively explains many of the effects observed during scanned cw laser crystallization, including periodic fluctuations in light emission. The second theoretical description is a more exact two-dimensional treatment applicable only to cases of steady-state motion of the *a-c* boundary, which can rigorously handle heat flow into the substrate. This treatment has been used to calculate the boundary velocity during steady-state runaway. The dependence of this velocity on background temperature and on film and substrate thermal properties and thickness has been determined from the theory. At the minimum background temperature required for runaway the calculated value of the steady-state velocity  $v_{ac}$  is  $\sim 140$  cm/sec for the case of a Ge film  $0.3\text{-}\mu\text{m}$  thick on a fused-silica substrate 1-mm thick. Experimental values for  $v_{ac}$  lie in the range 100–300 cm/sec. However, comparison of the theory with experiment suggests the presence of a thermal barrier between substrate and film, which would modify the theoretical results for  $v_{ac}$ . A class of laser-guided steady-state solutions has been obtained for which the boundary velocity is equal to the laser scanning velocity but lower than the boundary velocity for uncontrolled runaway.

### I. INTRODUCTION

The study of the transformation of semiconductor films from the amorphous to the crystalline state has become a matter of great interest in the last few years. The time dependence of the transformation has been investigated as a function of film temperature for Ge (Ref. 1) and Si (Ref. 2), and the latent heat of transformation and transformation temperature have been measured for Ge,<sup>3,4</sup> Si,<sup>4</sup> and Ge-Si alloys.<sup>4</sup> The so-called “explosive” transformation of semiconductor films as well as periodic features in films have been reported by a number of workers,<sup>5</sup> and the velocity of the transformation has been measured.<sup>6</sup>

We have recently reported the observation of a number of unusual phenomena during a study of the laser crystallization of amorphous Ge films.<sup>7</sup>

These phenomena included the formation of periodic structural features, pulsations of film temperature during laser scanning, and runaway crystallization of the entire film following momentary contact with the laser image. To provide a qualitative description of the laser-crystallization process, we presented a one-dimensional integral-equation description of the amorphous-crystalline (*a-c*) phase-boundary motion,<sup>8</sup> which takes into account the latent heat emitted during the *a-c* transformation. Numerical solution of the integral equation provides considerable insight into the dynamics of the *a-c* boundary. The results were used to obtain a semiquantitative fit of the temperature dependence of the structural periodicity observed in crystallization of amorphous Ge films on fused-silica substrates.

In this paper we present a somewhat improved

version of the one-dimensional integral-equation description of laser crystallization which takes account of the loss of heat to the film substrate by introducing into the equation an *ad hoc* exponential time-dependent damping factor. The results obtained for the motion of the *a-c* boundary are qualitatively very similar to those obtained earlier.<sup>8</sup> The solution of the integral equation is used to obtain series of plots of temperature as a function of lateral position in the film at fixed times after the onset of the crystallization process. These plots provide an understanding of the temperature pulsations during the formation of periodic structures in film morphology, as well as a vivid picture of the onset of *a-c* phase-boundary runaway. The general features of the model are strongly supported by our recent experimental study of *a-c* boundary dynamics during laser crystallization.<sup>9</sup>

The solutions of the one-dimensional integral equation provide an approximate description of transient as well as steady-state behavior of the *a-c* phase boundary motion. On the other hand, we have obtained a class of less approximate two-dimensional solutions which are stationary in a frame of reference moving with the *a-c* boundary. These solutions are exact if the temperature dependence of film and substrate properties as well as differences in amorphous and crystalline properties are neglected. The solutions allow a calculation of the *a-c* runaway boundary velocity. The runaway velocities calculated are in reasonable agreement with observation. The existence of laser-guided motion at a lower velocity is predicted by the two-dimensional calculations.

In Sec. II of this paper we present the transient and periodic steady-state solutions of the one-dimensional integral equation description of laser crystallization. The results of the model are compared to experimental results for laser crystallization of *a-Ge*. In Sec. III we obtain and compare the steady-state runaway solutions of the integral-equation approximation and the two-dimensional model. In Sec. IV we consider steady-state laser-guided solutions obtained from the integral-equation approximation and the two-dimensional model. Section V contains a discussion of possible improvement of the theoretical descriptions, more detailed considerations of film morphology produced by laser crystallization, and speculation on the possibility of achieving laser-guided crystallization at reduced scanning velocity. Some details of the calculations are omitted and are included in an unpublished work.<sup>10</sup>

## II. TRANSIENT AND PERIODIC SOLUTIONS OF THE INTEGRAL EQUATION

### A. Derivation of the integral equation

When the temperature of an amorphous semiconductor film is raised, transformation to the stable crystalline form takes place at a rate that increases exponentially with temperature,<sup>1,2</sup> so that over a narrow temperature interval at a temperature  $\sim T_c$  the ratio of the time required for transformation to the time required for a laser scan changes from  $\gg 1$  to  $\ll 1$ . We therefore argue that a reasonable description of the transformation is given by assuming that it occurs when the amorphous film reaches a critical temperature  $T_c$ . Support for this point of view comes from the observation of a rather sharply defined transformation temperature in latent-heat measurements.<sup>4</sup> It has been suggested<sup>11</sup> that the transformation may in fact correspond to the change from the amorphous to the liquid state, followed by a transformation to the crystalline state. In this case, the existence of a well-defined critical temperature  $T_c$  is expected. Therefore the assumption of a transformation at a constant temperature  $T_c$  should be a reasonable approximation in either case, and is justified by the good description of experiment that results. The modification of this assumption and the detailed nature of the transformation are considered further in the discussion of Sec. V.

We assume that the temperature dependence of the film properties and the difference in these properties between the amorphous and crystalline states can be neglected. This is an acceptable approximation at temperatures in the range of the amorphous-crystalline transformation ( $\sim 500-700^\circ\text{C}$  for Ge). With these simplifying assumptions, an integral-equation formalism<sup>12</sup> can be used to describe the motion of the phase boundary. The geometry assumed for the laser-crystallization calculation is shown schematically in Fig. 1. The semiconductor film, which is deposited on a thick substrate, is of infinite extent in the *y* and *z* directions and so thin that its temperature is constant in the *x* direction. The laser-slit image is of infinite length in the *z* direction and moves at a velocity *v* in the positive *y* direction. At time  $t=0$ , the phase boundary is located at  $y_0$ , with the crystalline phase to the left ( $y < y_0$ ) and the untransformed amorphous phase to the right ( $y > y_0$ ). The laser image carries with it a steady-state temperature profile  $T_0(y-vt)$ . At  $t=0$ , the

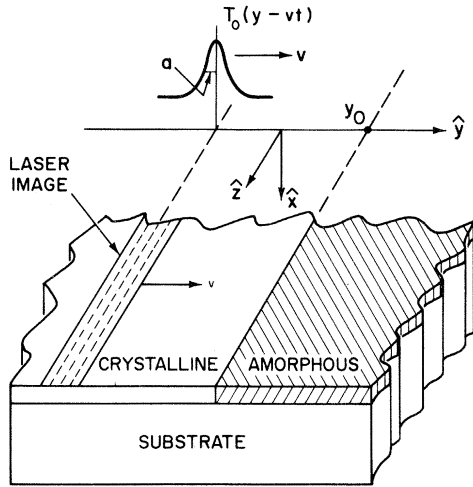


FIG. 1. Schematic representation of laser-crystallization experiment.

temperature at the phase boundary reaches  $T_c$  and the boundary begins to move irreversibly toward the right, with heat being liberated at a rate per boundary unit cross-section area of  $fL\rho\dot{Y}(t)$ , where

$L$  is the latent heat of  $a$ - $c$  transformation of the semiconductor,  $\rho$  is the semiconductor density,  $Y(t)$  is the position of the boundary at time  $t$ , and  $\dot{Y}(t)$  is its velocity. We have included a factor  $f$  which is less than 1 and accounts in an approximate way for the loss of a fraction  $(1-f)$  of the latent heat to the substrate as it is liberated. In the present version, we will also include an exponential damping factor  $\gamma$  to represent the eventual diffusion into the substrate of the fraction  $f$  of the heat propagating in the film. We shall see that  $f$  and  $\gamma$ , which are introduced as *ad hoc* parameters in the one-dimensional integral equation, have their counterparts in the two-dimensional steady-state model (Sec. III B), where they are determined in the course of the calculation, leaving no adjustable parameters. The effect of strain and other mechanical forces is not explicitly included, although  $L$  could include a contribution due to strain. Then the temperature  $T(y,t)$  at any point  $y$  along the film at time  $t$  is given by the one-dimensional integral relation<sup>12</sup>

$$T(y,t) = T_0(y-vt) + \frac{fL}{C} \int_0^t \dot{Y}(t') \{ \exp[-\gamma(t-t')] \} \left[ \exp\left\{ \frac{-[y-Y(t')]^2}{4\kappa(t-t')} \right\} \right] (4\pi\kappa)^{-1/2} (t-t')^{-1/2} dt', \quad (1)$$

where  $C$  is the specific heat of the film,  $\kappa = K/C\rho$  defines its thermal diffusivity,  $K$  is its thermal conductivity, and  $\gamma$  is a phenomenological damping factor.

Equation (1) has a simple physical interpretation. It states that the temperature at a point  $y$  at time  $t$  is a superposition of the contribution due to the moving laser,  $T_0(y-vt)$ , and the sum of contributions due to sources of heat  $fL\rho\dot{Y}(t')dt'$ , emitted at positions  $Y(t')$  at earlier times  $t'$ . The source function or Green's function

$$\left[ \exp\left\{ \frac{-[y-Y(t')]^2}{4\kappa(t-t')} \right\} \right] (4\pi\kappa)^{-1/2} (t-t')^{-1/2},$$

describes the one-dimensional diffusion of heat away from the source, and the factor  $\exp[-\gamma(t-t')]$  represents the decay of heat out of the film and into the substrate.

An integral equation for  $Y(t)$  can be obtained by using the condition that the temperature at the phase boundary is  $T_c$ , or

$$T[Y(t),t] = T_c. \quad (2)$$

For purposes of calculation, it is convenient to rewrite Eq. (2) in the frame of reference moving with the laser image. We introduce the position variable  $u(t) = y(t) - vt$ , where  $u(t)$  is measured from the center of the laser image as origin. The temperature  $T_0(u)$  is modeled in the form  $T_0(u) = T_b + \Delta T_l \exp[-(u/a)^2]$ , where  $T_b$  is a uniform, time-independent background temperature and the temperature contribution due to the laser is described by a Gaussian of width  $a$  and magnitude  $\Delta T_l$ . Finally, introducing normalized quantities with  $a$  as the unit of length, we can write the integral equation for the motion of the phase boundary as

$$1 = \alpha \exp\{-[S(\tau)]^2\} + \eta \int_0^\tau \{ [\dot{S}(\tau') + V]/(\tau-\tau')^{1/2} \} \{ \exp[-\Gamma(\tau-\tau')] \} \{ \exp\{-[S(\tau)-S(\tau') + V(\tau-\tau')]^2/(\tau-\tau')\} \} d\tau' \quad (3)$$

where

$$\alpha = \Delta T_l / (T_c - T_b), \quad (4a)$$

$$\eta = f\eta', \quad \eta' = L / C\pi^{1/2}(T_c - T_b), \quad (4b)$$

$\tau \equiv 4\kappa t / a^2$ ,  $V \equiv av / 4\kappa$ ,  $S \equiv U / a$ ,  $\dot{S}(\tau') \equiv dS(\tau') / d\tau'$ ,  $\Gamma = (a^2 / 4\kappa)\gamma$ , and  $U$  is the position of the phase boundary measured from the center of the laser image.

Equation (3) is not in itself sufficient to give physically acceptable solutions for the motion of the phase boundary, since it allows negative values of  $S(\tau') + V$ , which imply the unphysical motion of the phase boundary back toward the laser image, with the reconversion of crystalline material to the amorphous state, accompanied by the reabsorption of latent heat. To constrain Eq. (3) to physically acceptable solutions, we require that when the numerical solution of Eq. (3) yields  $S(\tau') + V \leq 0$ , this quantity is to be set equal to zero, with the phase boundary remaining stationary.

Equation (3) has been solved numerically<sup>10</sup> to obtain  $S$  as a function of  $\tau$  for representative values of  $\alpha$ ,  $\eta$ ,  $V$ , and  $\Gamma$ , with the boundary conditions that  $S(\tau) = 0$  at  $\tau = 0$  and that  $S(0)$  is given by  $1 = \alpha \exp\{-[S(0)]^2\}$ . The values of the parameters have been chosen for convenience in numerical solution of Eq. (3) rather than an optimal fit to experimental conditions. Figure 2 shows plots of  $S$  vs  $\tau$  for  $V = 0.3$ ,  $\Gamma = 30$  and three increasing values of  $\eta$ , with  $\alpha$  increasing in proportion to  $\eta$  [which corresponds, from Eqs. (4a) and

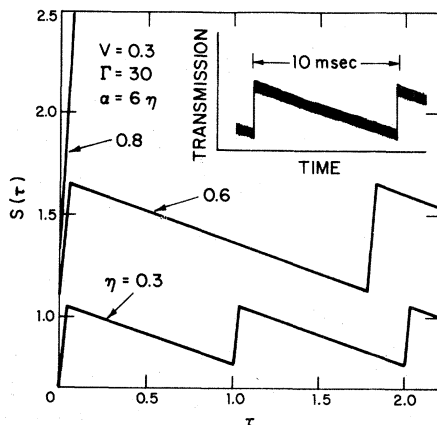


FIG. 2. Normalized position of  $a$ - $c$  phase boundary with respect to center of laser thermal image  $S(\tau)$  as a function of normalized time  $\tau$  given by solutions of Eq. (3) for three different values of  $\eta$ . The inset shows the result of an experiment in which change of transmission is proportional to  $S(\tau)$ .

(4b), to increasing  $T_b$  toward  $T_c$  while holding  $\Delta T_l$  fixed.] For each value of  $\eta$ ,  $S$  initially increases rapidly because the latent heat liberated by the phase transformation raises the temperature ahead of the boundary, accelerating its forward motion. As the boundary moves away from the laser image, the contribution of the laser to the temperature ahead of the boundary decreases rapidly. For  $\eta = 0.3$ , the boundary motion soon decelerates, and the boundary comes to rest, remaining fixed for a time interval during which its temperature begins to drop rapidly below  $T_c$  and  $S$  decreases with velocity  $S = -V$ . With the approach of the laser image the boundary temperature gradually increases to  $T_c$ , the boundary once more moves forward, and  $S$  again increases. This cycle is repeated indefinitely, resulting in the oscillations in  $S$  seen for  $\eta = 0.3$  in Fig. 2. The inset in Fig. 2 shows the result of an experiment<sup>9</sup> which measures the infrared light transmitted through a thin film of Ge as the  $a$ - $c$  boundary moves in a cw laser-crystallization experiment. Since the transmission of crystalline Ge is much greater than that of amorphous Ge, the changes in transmitted light signal with time are proportional to the  $a$ - $c$  boundary position with time. The similarity between the oscillations observed in the experiment and those shown in the curve for  $\eta = 0.3$  is evident.

When  $\eta$  is increased by increasing  $T_b$ , less heat is required to raise the temperature of the film to  $T_c$  ahead of the laser image, and the phase boundary moves farther beyond the laser before it decelerates and comes to rest. This trend is illustrated by the calculated curve for  $\eta = 0.6$  in Fig. 2 and leads to motion with a longer period. When  $\eta$  becomes large enough, the heat liberated during crystallization is sufficient to sustain the transformation, causing the boundary to "run away" from the laser image. This situation, which is illustrated by the curve for  $\eta = 0.8$  in Fig. 2, accounts for the observation that for high enough background temperature the entire film is crystallized following momentary contact with the laser image.

In addition to explaining runaway crystallization, the proposed model can also explain our other qualitative observations on laser crystallization. The model does not directly predict observable structural changes in the laser-treated films. However, different regions of such films can be expected to differ in microstructure depending on their rates of transformation and therefore on their thermal history. This suggests that the periodic structural features observed on laser-crystallized films

(see Figs. 3 and 4) can be attributed to oscillations in  $S$  like those implied by the curves for  $\eta=0.3$  and 0.6 in Fig. 2. Furthermore, for sufficiently high values of  $\eta$  these oscillations produce large fluctuations in the rate of heat liberation and therefore in temperature. This can explain the periodic fluctuations in light emission observed during some laser-crystallization experiments (see Sec. II C).

### B. Comparison with experiment

In order to carry out a semiquantitative test of the model, we have measured the spatial period of the structural features of laser-crystallized Ge films as a function of  $T_b$ .<sup>7</sup> Experiments were performed on amorphous films 0.3- $\mu\text{m}$  thick, deposited on fused-silica substrates and scanned at  $v=0.5$  cm/sec with a slit image of a cw Nd:YAG (yttrium aluminum garnet) laser. Initially, a film at room temperature was irradiated at a laser power level just high enough to produce crystallization, which yielded structure in the transformed film with a spatial period of  $\sim 50 \mu\text{m}$ . In the following experiments each film was heated to a successively higher value of  $T_b$ , the laser scanned at the same power level, and the spacing measured after crystallization. This procedure was continued until

$T_b$  approached the value resulting in runaway.

The periodic features obtained by crystallization of a film with  $T_b$  of room temperature are shown in Fig. 3, an optical transmission micrograph. These features are shown at higher magnification by the left side of Fig. 4, which is a bright-field micrograph obtained by transmission electron microscopy (TEM) using 125-keV electrons. Each feature consists of four different regions: first a narrow amorphous region, then a region containing a mixture of amorphous material and fine grains, next a broad region of fine grains, and finally another broad region of much larger, elongated crystallites aligned parallel to each other. The fine-grained region yields transmission-electron diffraction patterns like the one shown at the upper right of Fig. 4, with the rings typical of polycrystalline material. The large crystallites of the final region are clearly visible as ribbonlike structures in the lower left corner of the TEM micrograph, and yield characteristic single-crystal transmission electron diffraction patterns, as illustrated at the lower right of Fig. 4. It should be emphasized that these large aligned crystallites are produced without the presence of a relief structure in the amorphous-silica substrate.<sup>13</sup> The nature of the crystalline structure within each period is discussed further in Sec. V.

To use the model to calculate the spatial period

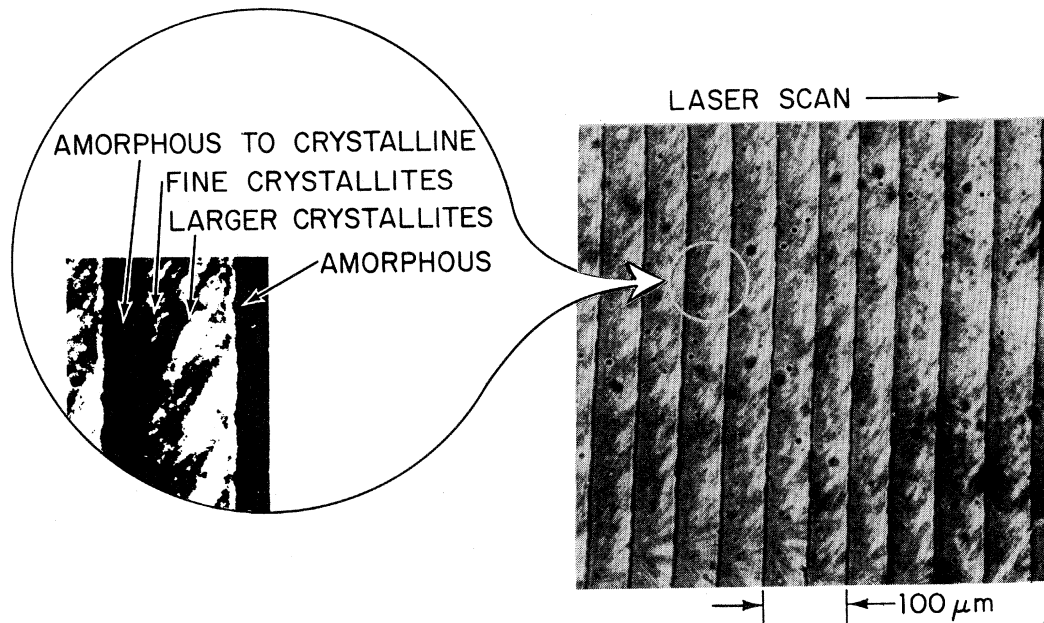


FIG. 3. Optical transmission micrograph of a laser-crystallized Ge film showing periodic structural features. Inset is expanded view illustrating four different microstructure regions.

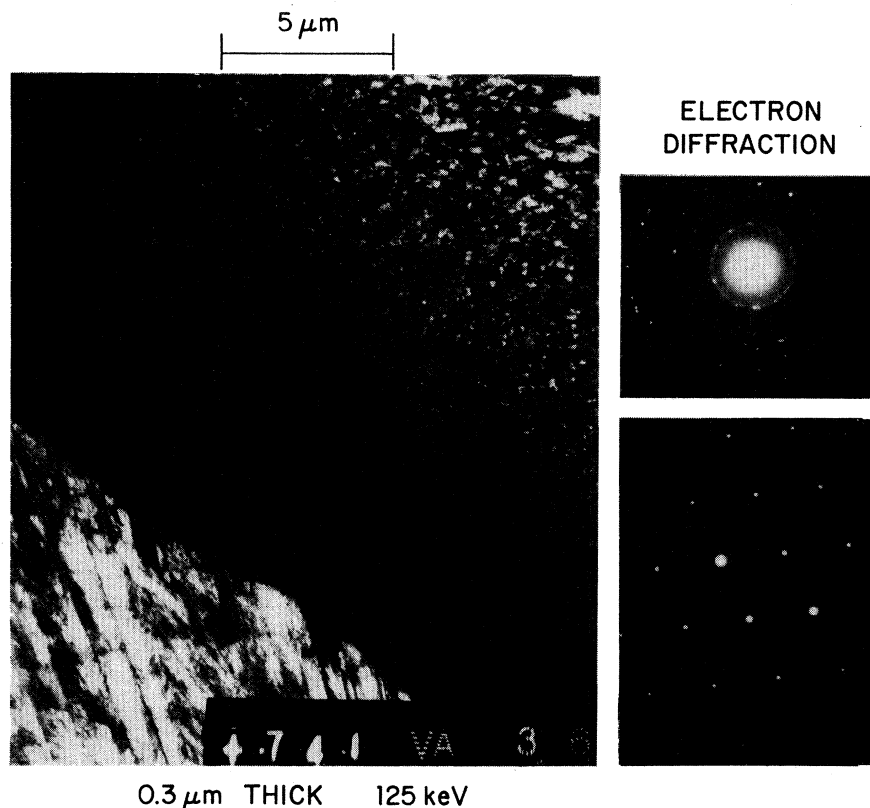


FIG. 4. Left: Bright-field transmission-electron micrograph of a laser-crystallized Ge film, illustrating four different microstructure regions. Right: Transmission-electron diffraction patterns for fine-grained and large-grained regions (upper and lower, respectively).

in the film, we assume that this period is equal to the distance  $\Delta Y$  traversed by the  $a$ - $c$  phase boundary during each of its successive jumps, from the point where crystallization is initiated by the approaching laser to the point where the boundary comes to rest ahead of the laser. This distance is just equal to  $aV\Delta\tau$ , where  $V$  is the normalized laser-scanning velocity and  $\Delta\tau$  is the normalized time interval between the beginnings of two successive jumps, i.e., the period of the oscillations in  $S$  illustrated by the curves for  $\eta=0.3$  and  $0.6$  in Fig. 2.

To obtain a relationship between  $\Delta Y$  and  $T_b$ , we first used Eq. (3) to calculate  $V\Delta\tau$  as a function of  $\eta$  for representative values of  $\alpha$ ,  $V$ , and  $\Gamma$ . Because of the introduction of the new damping parameter  $\Gamma$ , the results obtained are numerically somewhat different from those reported earlier,<sup>7,8</sup> but are qualitatively unchanged. The calculated curve for  $\alpha=6\eta$  (corresponding to fixed  $\Delta T_l$ ,  $V=0.3$ , and  $\Gamma=30$ ) is shown in Fig. 5. With increasing  $\eta$ ,  $\Delta\tau$  and therefore  $V\Delta\tau$  increase rapidly,

leading to boundary runaway by  $\eta\approx 0.69$ . For a given value of  $\eta$ ,  $V\Delta\tau$  is found to be quite insensitive to either  $\alpha$  or  $V$ , showing that the boundary-jump distance is determined primarily by the properties of the film and by  $T_b$ , and does not depend strongly on either the power or velocity of the laser.

In order to compare theory with experiment, the curve of  $V\Delta\tau$  vs  $\eta$  shown in Fig. 5 was used to obtain curves relating the ratios  $\Delta Y/\Delta Y_0$  and  $T_b/T_c$ , where  $\Delta Y_0$  is the spatial period in the film (i.e., the boundary-jump distance) for  $T_b$  of room temperature. To calculate these curves, Eq. (4b) was rewritten in the lumped-parameter form  $\eta = \eta_0 / (1 - T_b/T_c)$ , where  $\eta_0 \equiv fL / \pi^{1/2} CT_c$ . When  $T_b$  and  $T_c$  are expressed in  $^{\circ}\text{C}$ , room temperature is much less than  $T_c$ , so that  $\eta_0 \approx \eta$  at room temperature, and  $\Delta Y_0$  corresponds to  $\eta_0$ . Curves of  $\Delta Y/\Delta Y_0$  vs  $T_b/T_c = 1 - \eta_0/\eta$  were calculated by adopting pairs of numerical values of  $\eta_0$  and  $T_c$ , then compared with the experimental points (for each point, the adopted value of  $T_c$  was

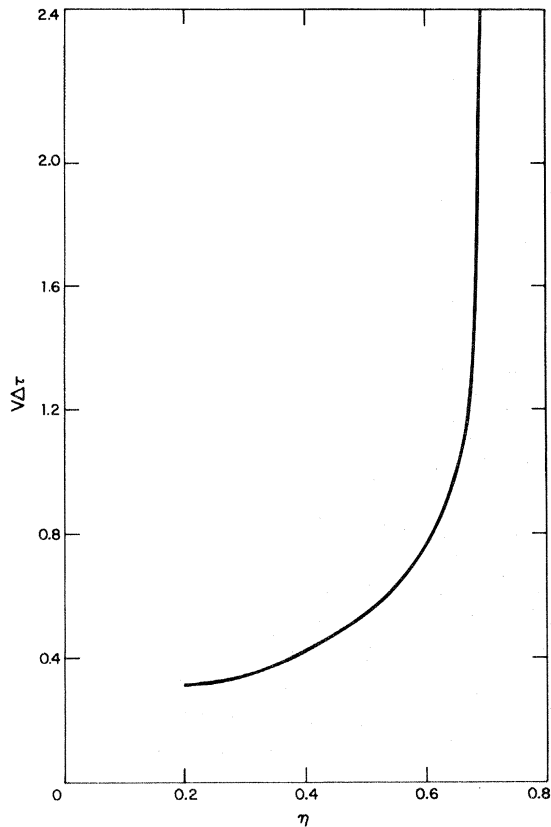


FIG. 5.  $V\Delta\tau$  vs  $\eta$  from solutions of Eq. (3).

used to determine  $T_b/T_c$ ). A reasonable overall fit has been obtained, as shown in Fig. 6, for  $\eta_0 \approx 0.22$  and  $T_c \approx 680^\circ\text{C}$ . The abrupt increase in  $\Delta Y/\Delta Y_0$  when  $T_b/T_c$  exceeds about 0.6 is associated with the approach of  $T_b$  to the value  $T_r$  above which laser irradiation results in boundary runaway. From Fig. 6, we note that  $T_r \sim 0.7T_c$ , and using  $T_c \sim 680^\circ\text{C}$  we find  $T_r \cong 500^\circ\text{C}$ . It is interesting to note that Bagley and Chen<sup>11</sup> predict a transformation of *a*-Ge to the liquid state at a temperature of  $696^\circ\text{C}$ , well below the crystalline-to-liquid transition temperature ( $937^\circ\text{C}$ ), and close to the value of  $\sim 680^\circ\text{C}$  obtained from our analysis.

From the definition of  $\eta_0$ ,  $fL = \pi^{1/2}CT_c\eta_0$ . Taking  $C = 0.08$  cal/g $^\circ\text{C}$  for amorphous Ge (Ref. 3) and the values of  $T_c$  and  $\eta_0$  used for Fig. 6, we obtain  $fL = 21.4$  cal/g. In calorimetric measurements made during the rapid heating of amorphous Ge films, Fan and Anderson<sup>4</sup> observed a sharp transition at  $\sim 501^\circ\text{C}$  and measured  $L = 39.8$  cal/g. Using this value for  $L$  yields the result  $f \sim 0.54$ . The value of  $f$  obtained seems large, unless a thermal barrier impedes transfer of heat from the film to the substrate (see Sec. III B).

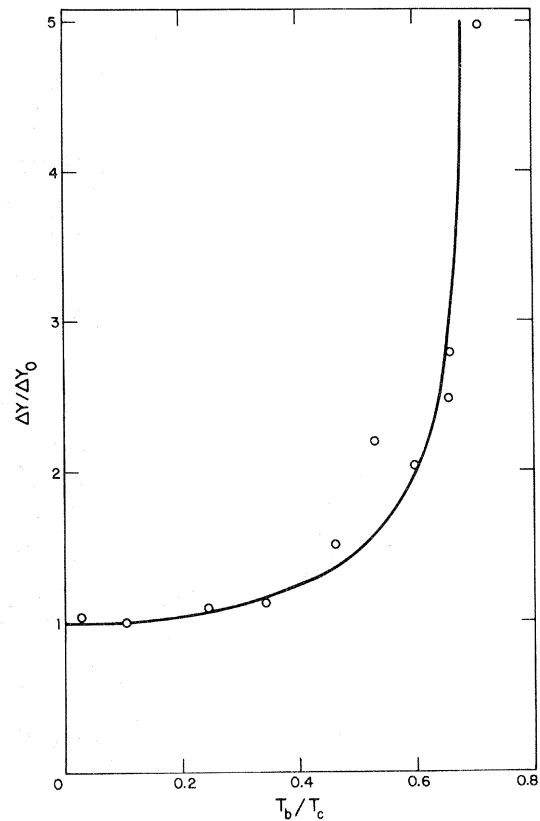


FIG. 6. Theoretical curve and experimental points for  $\Delta Y/\Delta Y_0$  vs temperature ratio  $T_b/T_c$ . Curve is calculated using Fig. 5 with  $\eta_0 = 0.22$  and  $T_c = 680^\circ\text{C}$ .

The values of  $S(\tau)$  plotted in Fig. 2 for the regions in which the phase boundary moves away from the laser image are not quantitatively correct, since the calculated values of  $S$  in this region increase more steeply as the size of the interval  $\delta\tau$  chosen for the numerical integration of Eq. (3) is decreased. An examination of the integral equation indicates that in the beginning of these regions its solutions is singular and the initial velocity is infinite. This represents a limitation of the model since we have implicitly assumed that growth of the crystalline phase can follow at all times the requirements of the solution of the heat-flow problem. In fact, the failure of this assumption may account for the presence of amorphous and fine-grained material in the initial portion of each periodic feature of the laser-crystallized films. However, since the calculated values of  $S$  at which the boundary comes to rest approach a limit as  $\delta\tau$  decreases, the computed spatial periods are reasonably reliable.

The Gaussian width of the temperature profile

due to the laser can be determined from the relationship  $a = \Delta Y / V \Delta \tau$ . From the measured  $\Delta Y_0 = 50 \mu\text{m}$  at room temperature and  $V \Delta \tau \approx 0.3$  corresponding to  $\eta_0 = 0.22$  in Fig. 5,  $a$  is  $\sim 170 \mu\text{m}$ , a reasonable value. The scanning velocity  $v$  corresponding to the normalized velocity  $V$  in our calculation can be obtained by using the relation  $v = 4\kappa V / a$ . A value for  $\kappa$  of  $\sim 0.09 \text{ cm}^2/\text{sec}$  is estimated by taking  $K = 0.035 \text{ cal/cm sec } ^\circ\text{C}$  (Ref. 14),  $\rho \sim 5 \text{ g/cm}^3$ , and  $C = 0.08 \text{ cal/g } ^\circ\text{C}$ . The value of normalized laser-scan velocity used in our calcu-

lations, which was chosen for convenience in numerical integration, was  $V = 0.3$ . This corresponds to a laser-scan velocity  $v$  of  $\sim 6 \text{ cm/sec}$ , much higher than the actual value of  $0.5 \text{ cm/sec}$  used in our experiments. As indicated above, the results of our analysis of periodic  $a$ - $c$  boundary motion are insensitive to the value of  $v$  assumed for the calculation as long as  $v$  is much less than the boundary velocity  $v_{ac}$ . For both runaway<sup>6</sup> and periodic motion<sup>9</sup> of the boundary, experimental values of  $v_{ac}$  lie in the range of  $100$ – $300 \text{ cm/sec}$ .

### C. Temperature distribution during periodic boundary motion

Once the  $a$ - $c$  boundary position as a function of time,  $S(\tau)$ , is known, Eq. (1) can be used to calculate the temperature at an arbitrary point  $S'$  in the film at time  $\tau$ . The resulting expression for the reduced temperature in terms of normalized quantities in the frame of reference moving with the laser is

$$T'(S', \tau) = \alpha \exp[-(S')^2] + \eta \int_0^\tau \{ [\dot{S}(\tau') + V] / (\tau - \tau')^{1/2} \times \{ \exp[-\Gamma(\tau - \tau')] \} (\exp\{-[S' - S(\tau') + V(\tau - \tau')]^2 / (\tau - \tau')\}) d\tau', \quad (5)$$

where the reduced temperature is

$$T'(S', \tau) \equiv \frac{T(S', \tau) - T_b}{T_c - T_b}.$$

It can be seen that when  $S'$  is the position of the  $a$ - $c$  boundary,  $S(\tau)$ ,  $T(S', \tau) = T_c$ ,  $T'(S', \tau) = 1$ , and Eq. (5) becomes the integral equation (3). The numerical evaluation of Eq. (5) is discussed in Ref. 10.

To illustrate the fluctuations occurring in temperature and light emission during periodic boundary motion, we have used Eq. (5) to calculate  $T'(S', \tau)$  as a function of  $S'$  for several fixed values of  $\tau$ , for the case  $\alpha = 1.2$ ,  $\eta = 0.6$ ,  $V = 0.3$ , and  $\Gamma = 30$ . The results are shown in Fig. 7. It can be seen that during the forward motion of the  $a$ - $c$  phase boundary, a temperature pulse develops and propagates away from the center of the temperature profile due to the laser. Before the pulse can escape, however, its motion stalls and it decays. In this case the laser temperature contribution is just barely large enough to initiate  $a$ - $c$  boundary motion, and the latent heat released is enough to cause a sharp rise in temperature accompanied by the emission of black-body visible radiation. The peak temperature  $T_p$  reached can be calculated for this example by noting that

$$T_p = T_b + T'_p(T_c - T_b), \quad (6)$$

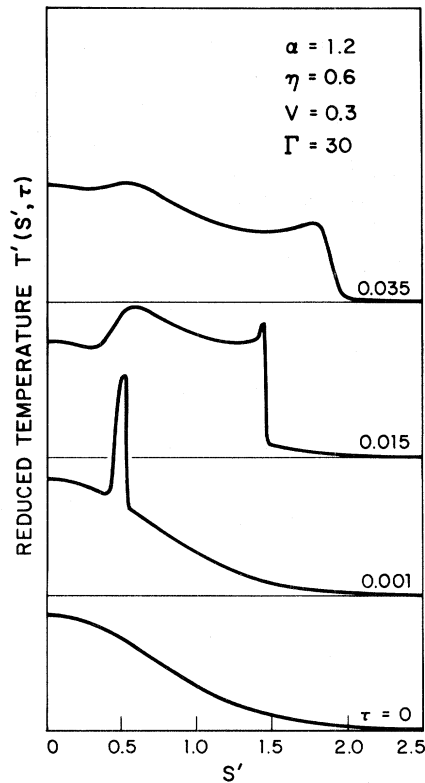


FIG. 7. Normalized temperature distribution  $T'(S', \tau)$  as a function of  $S'$  for several values of  $\tau$ , illustrating periodic fluctuations in temperature and light emission.

where  $T'_p$  is the peak value reached in Fig. 7. Equation (6) can be rewritten

$$T_p = T_c \left[ \left[ 1 - \frac{\eta_0}{\eta} \right] + T'_p \left[ \frac{\eta_0}{\eta} \right] \right].$$

Using  $T_c = 680^\circ\text{C}$ ,  $\eta_0 = 0.22$ ,  $\eta = 0.6$ , and  $T'_p \approx 2.2$ , we have  $T_p \approx 986^\circ\text{C}$ . Although the numerical result is only approximate (since the computed velocity of the  $a$ - $c$  boundary depends on the time interval  $\delta\tau$  chosen for numerical integration), the calculation indicates that a large rise in temperature, and therefore light emission, can occur during  $a$ - $c$  boundary motion.

### III. STEADY-STATE RUNAWAY SOLUTIONS

#### A. Integral-equation model

As we have seen in Sec. II A, for large enough values of  $\eta$  and relatively small values of normalized laser-scan velocity  $V$ , the solutions of Eq. (3) are of the runaway type with the  $a$ - $c$  boundary escaping from the region of the laser image and moving far ahead of it. In this case, Eq. (3) can be solved exactly without the need for numerical integration, by making the assumption that a steady-state, constant-velocity solution exists after the passage of a long enough time  $\tau_0$ . For the boundary far ahead of the laser image the laser contribution to Eq. (3) is negligible. We rewrite Eq. (3) at time  $\tau_0$  in the frame of reference moving with the boundary at the normalized velocity  $V_{ac} \gg V$ , with  $V_{ac}$  to be determined. In this frame of reference,  $V$  is replaced by  $V_{ac}$ ,  $S(\tau) = S(\tau')$ , and  $S(\tau') = 0$  (since the solution is stationary). Equation (3) then becomes

$$1 = \eta \int_0^{\tau_0} [V_{ac}/(\tau - \tau')^{1/2} \{ \exp[-\Gamma(\tau - \tau')] \} \times (\exp\{ -[V_{ac}(\tau - \tau')]^2 / (\tau - \tau') \})] d\tau'. \quad (7)$$

Introducing the new variable  $z^2 \equiv (\Gamma + V_{ac}^2)(\tau - \tau')$ , Eq. (7) can be rewritten as

$$1 = \eta \frac{V_{ac}}{(\Gamma + V_{ac}^2)^{1/2}} 2 \int_0^{(\Gamma + V_{ac}^2)^{1/2} \tau_0^{1/2}} e^{-z^2} dz \\ = \eta \pi^{1/2} \frac{V_{ac}}{(\Gamma + V_{ac}^2)^{1/2}} \operatorname{erf}[(\Gamma + V_{ac}^2)^{1/2} \tau_0^{1/2}], \quad (8)$$

where

$$\operatorname{erf}(x) = \frac{2}{\sqrt{\pi}} \int_0^x e^{-z^2} dz$$

is the error function. The error function approaches 1 for  $x \gtrsim 2$ . Therefore, for

$$(\Gamma + V_{ac}^2)^{1/2} \tau_0^{1/2} > 2,$$

Eq. (8) reduces to

$$1 = \eta \pi^{1/2} \frac{V_{ac}}{(\Gamma + V_{ac}^2)^{1/2}}. \quad (9)$$

Equation (9) can be used to determine the runaway  $a$ - $c$  boundary velocity  $V_{ac}$  from the values of  $\eta$  and  $\Gamma$ :

$$V_{ac} = \frac{\Gamma^{1/2}}{(\eta^2 \pi - 1)^{1/2}}. \quad (10)$$

It can be seen that Eq. (10) has no solution for any value of  $V_{ac}$ , no matter how large, unless  $\eta \pi^{1/2} > 1$ , or  $\eta > 0.56$ .

In the runaway case, Eq. (5) for the reduced temperature distribution can also be evaluated exactly for large  $\tau_0$ . In the same frame of reference moving with normalized velocity  $V_{ac}$ , Eq. (5) becomes

$$T'(S') = \eta \int_0^{\tau_0} [V_{ac}/(\tau - \tau')^{1/2} \{ \exp[-\Gamma(\tau - \tau')] \} \times (\exp\{ -[S' + V_{ac}(\tau - \tau')]^2 \} \times 1(\tau - \tau'))] d\tau', \quad (11)$$

where  $S'$  is measured from the position of the  $a$ - $c$  phase boundary. Equation (11) can be written

$$T'(S') = \eta \frac{V_{ac}}{(\Gamma + V_{ac}^2)^{1/2}} 2 \exp(-2S'V_{ac}) \times \int_0^{(\Gamma + V_{ac}^2)^{1/2} \tau_0^{1/2}} e^{-z^2} e^{-q^2/z^2} dz, \quad (12)$$

where  $q^2 = S'^2(\Gamma + V_{ac}^2)$ . Using the known definite integral,

$$\int_0^\infty e^{-p^2 z^2} e^{-q^2/z^2} dz = \frac{\sqrt{\pi}}{2p} e^{-2pq} \quad (p, q > 0)$$

we obtain, for large  $\tau_0$ ,

$$T'(S') = \eta \pi^{1/2} \frac{V_{ac}}{(\Gamma + V_{ac}^2)^{1/2}} \exp(-2S'V_{ac}) \times \exp[-2(\Gamma + V_{ac}^2)^{1/2} |S'|]. \quad (13)$$

For  $S' = 0$ , corresponding to the position of the  $a$ - $c$  boundary,  $T'(S') = 1$ , and Eq. (13) reduces to Eq. (9), as it should.

The expressions for the steady-state boundary velocity, Eq. (10), and the steady-state temperature distribution, Eq. (13), come from exact solutions of Eqs. (7) and (11), respectively. However, the approach to the steady state after excitation by a cw laser can only be studied by numerical integration of Eqs. (3) and (5). To explore the approach to the steady-state runaway temperature distribution, we have used the values of  $S(\tau)$  obtained from numerical integration of Eq. (3) for  $\alpha=2.0$ ,  $\eta=0.8$ ,  $V=0.3$ , and  $\Gamma=30$ , to calculate  $T'(S',\tau)$  from Eq. (5) for several values of  $\tau$ . The results are shown in Fig. 8. In contrast to the periodic solution case shown in Fig. 7, the  $a$ - $c$  boundary in the runaway case develops a well-defined peak structure in  $T'(S',\tau)$ , which propagates away from the laser image as  $\tau$  increases. The velocity of propagation of the  $a$ - $c$  boundary and the amplitude and shape of the propagating temperature pulse shown in Fig. 8 are in qualitative agreement with the exact limiting results given by Eqs. (10) and (13), respectively. However, the quantitative agreement is not good. Thus, from Eq. (10) with  $\Gamma=30$  and  $\eta=0.8$  we have the exact result  $V_{ac}=5.45$ , much less than the velocity obtained from Fig. 8. The discrepancy may in part be due to computational problems, but may also be due to a slow approach to the steady state. [It should be noted that at the maximum  $S(\tau)$  shown, the  $a$ - $c$  boundary has moved only a few times the Gaussian width,  $\sim 170 \mu\text{m}$ , from the laser beam.]

The exact solution for the steady-state velocity  $V_{ac}$ , given by Eq. (10), decreases as the value of  $\eta$  increases. Similar behavior for the steady-state boundary velocity is found from the solution of a two-dimensional heat-flow problem discussed in the following subsection.

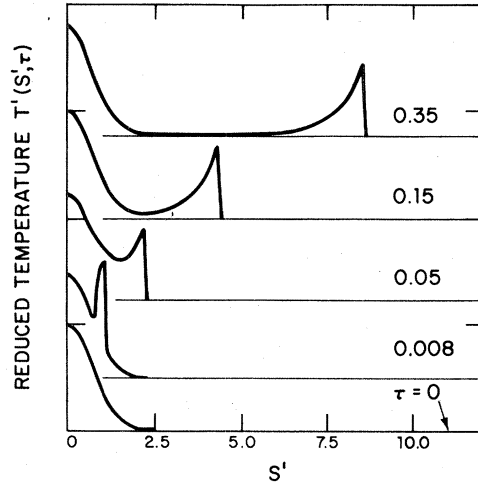


FIG. 8. Normalized temperature distribution  $T'(S',\tau)$  as a function of  $S'$  for several values of  $\tau$ . The parameter values  $\alpha=2.0$ ,  $\eta=0.8$ ,  $V=0.3$ ,  $\Gamma=30$  have been chosen to illustrate the case of runaway.

### B. Two-dimensional solution

We have obtained expressions for the temperature distribution in the steady-state  $a$ - $c$  boundary runaway condition for a semiconductor film as a function of normalized distance  $S'$  from the boundary by the solution of a two-dimensional boundary value problem.<sup>10</sup> In this treatment the flow of heat into the substrate is handled exactly, and it is not necessary to introduce *ad hoc* parameters equivalent to  $f$  and  $\gamma$  of the one-dimensional integral-equation model. The results give the temperature distribution in the semiconductor film of thickness  $b_1$  supported on a substrate of thickness  $b_2$  as a function of steady-state normalized velocity  $V_{ac}$  of the  $a$ - $c$  boundary. If the  $a$ - $c$  boundary is at the temperature  $T_c$ , then the expression obtained is<sup>10</sup>

$$T'(S') = \eta' V_{ac} \pi^{1/2} \sum_{n^+} \frac{e^{-2V_{ac}S'} e^{-2(\Gamma_{n^+} + V_{ac}^2)^{1/2}|S'|}}{(\Gamma_{n^+} + V_{ac}^2)^{1/2}} f_{n^+}(V_{ac}) \quad (S' < 0), \quad (14a)$$

$$T'(S') = \eta' V_{ac} \pi^{1/2} \sum_{n^-} \frac{e^{-2V_{ac}S'} e^{-2(\Gamma_{n^-} + V_{ac}^2)^{1/2}|S'|}}{(\Gamma_{n^-} + V_{ac}^2)^{1/2}} f_{n^-}(V_{ac}) \quad (S' > 0), \quad (14b)$$

where

$$T'(S') = \frac{T_1(S') - T_b}{T_c - T_b}, \quad \eta' = \frac{L}{\pi^{1/2} C_1 (T_c - T_b)}, \quad f_{n^\pm}(V) = \frac{1}{1 - \frac{\beta}{2} \left[ \frac{\cot Q_{n^\pm}}{Q_{n^\pm}} - \csc^2 Q_{n^\pm} \right] \left[ 1 \pm \frac{V(M-1)}{(\Gamma_{n^\pm} + V^2)^{1/2}} \right]}, \quad (14c)$$

where  $\beta = K_2 b_2 / K_1 b_1$  and  $M = \kappa_1 / \kappa_2$ , and  $S'$  is the normalized distance from the  $a$ - $c$  boundary, with normalization unit of length equal to  $b_2$ . Subscripts 1 and 2 refer to laser-crystallized film and substrate, respectively. The  $\Gamma_{n+}$  and  $\Gamma_{n-}$  are roots of a transcendental equation, and the  $Q_{n\pm}$  are given by expressions which are functions of  $\Gamma$  evaluated for  $\Gamma_{n\pm}$ .<sup>10</sup>

One case for which the solution of Eqs. (14a) and (14b) can be readily evaluated is a thin amorphous film on a thick substrate with identical thermal properties ( $M = 1$ ,  $\beta = b_2 / b_1 \gg 1$ ). For this case,  $f_{n+} = f_{n-} = 2/\beta$ ;  $\Gamma_{n+} = \Gamma_{n-} = (2n+1)^2 \pi^2 / 16$ .

The general condition determining the steady-state  $a$ - $c$  boundary velocity  $V_{ac}$  is that at  $S' = 0$ ,  $T'(0) = 1$  or,

$$1 = \eta' V_{ac} \pi^{1/2} \sum_{n+} \frac{f_{n+}(V_{ac})}{(\Gamma_{n+} + V_{ac}^2)^{1/2}} = \eta' V_{ac} \pi^{1/2} \sum_{n-} \frac{f_{n-}(V_{ac})}{(\Gamma_{n-} + V_{ac}^2)^{1/2}}. \quad (15)$$

It is interesting to compare the results of Eqs. (14a), (14b), and (15) with the one-dimensional integral-equation results of Eqs. (13) and (9), respectively. Noting that  $\eta = f\eta'$ , it can be seen that Eqs. (13) and (9) represent approximations in which single average terms have replaced sums of terms of the same form in the two-dimensional result.

We define the functions in the summation in Eqs. (14a) and (14b) as

$$F^{\pm}(S', V) \equiv \sum_{n\pm} \frac{e^{-2VS'} e^{-2(\Gamma_{n\pm} + V^2)^{1/2} |S'|}}{(\Gamma_{n\pm} + V^2)^{1/2}} f_{n\pm}(V). \quad (16)$$

$F^{\pm}(S', V)$  is proportional to the steady-state temperature distribution due to a slit-image source of heat scanned with normalized velocity  $V$  along the surface of a semiconductor film. When evaluated for  $V = V_{ac}$ , it yields the shape of the distribution for  $a$ - $c$  boundary runaway. We have evaluated Eq. (16) as a function of  $S'$  for a number of values of  $V$  for the case of a thin film of Ge on a fused-silica substrate, since the experimental results reported in Sec. IIB were obtained for this case. The values of  $K_1 = 0.035$  cal/cm sec °C,  $\kappa_1 = 0.09$  cm<sup>2</sup>/sec, and  $K_2 = 0.0025$  cal/cm sec °C,  $\kappa_2 = 0.005$  cm<sup>2</sup>/sec were those for Ge (1), and fused silica (2). The thicknesses used in the calculation, appropriate to our experiments<sup>7,8</sup> were  $b_1 = 0.3$   $\mu$ m for Ge and  $b_2 = 1$  mm for fused silica. With these values,  $\beta \cong 240$ , and  $M \cong 18$ .

Figure 9 shows  $F(S', V)$  as a function of  $S'$  for several values of  $V$ . For  $V \gtrsim 0.1$ , the leading edge of the temperature distribution begins to sharpen, and the peak value begins to drop. This is an indication that  $V$  has reached a value at which diffusion of heat can no longer restore the static temperature distribution as the heat source moves. It should also be noted that the fact the two portions of the curves of  $F^{\pm}(S', V)$  meet at  $S' = 0$  is a significant check on the correctness of the numerical calculation, since the formal expressions for  $[F^+(S', V)]_{S'=0}$  and  $[F^-(S', V)]_{S'=0}$  are not identical.

To obtain quantitative results for  $V_{ac}$ , we make

use of Eq. (15) and assume that  $T_c$  is a fixed transition temperature (modification of this assumption is discussed in Sec. V). The relation to be solved for  $V$  can be written,

$$\pi^{1/2} \eta' V_{ac} = [F(0, V_{ac})]^{-1}. \quad (17a)$$

We plot  $\log[F(0, V)]^{-1}$  vs  $\log V$  and  $\log(\pi^{1/2} \eta' V)$  vs  $\log V$  on the same graph. The solution for  $V_{ac}$  will be given by the intersection of the two curves. Figure 10 shows  $[F(0, V)]^{-1}$  for  $M = 18$  (corresponding to our experiments with  $a$ -Ge films on fused silica), and for several values of  $\beta$ . We

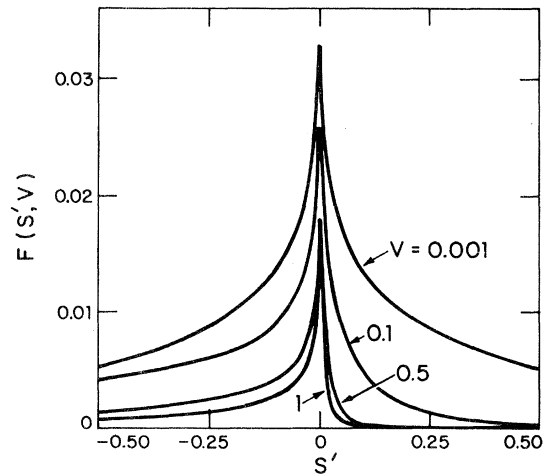


FIG. 9.  $F(S', V)$  as a function of  $S'$  for several values of  $V$ .

first consider the curve for  $\beta=240$ , corresponding to our experiment. One of the straight lines shown gives  $\log(\pi^{1/2}\eta'V)$  for  $\eta'=2.2$ , and we see that there is no solution for this value of  $\eta'$ . The minimum value of  $\eta'$  for a steady-state solution,  $\eta'_{\min}$ , corresponds to the lowest temperature ( $T_r$ ) at which runaway can occur. This solution is obtained when the two curves first cross, and is found to occur at  $\eta'_{\min}\cong 6.1$ . For values of  $\eta'$  greater than 6.1, there are steady-state runaway solutions for  $V_{ac}$  which decrease with increasing  $\eta'$ . It should be noted that the two curves first make contact tangentially as  $\eta'$  increases to  $\eta'_{\min}$ . This is similar to the integral-equation result, Eq. (10).

It is difficult to identify the first true "crossing" point for two curves that approach each other tangentially. Roughly, for  $\eta'\cong 6.1$  the two curves cease to run parallel for  $\log V\sim 1.6$ . Using the relation  $v\sim 4\kappa_1V/b_2$ , with  $\kappa_1=0.09$  cm<sup>2</sup>/sec, and  $b_2=10^{-1}$  cm, we find,  $v_{ac}\cong 140$  cm/sec. Larger values of  $\eta'$  should lead to smaller values of  $v_{ac}$ , consistent with the integral-equation result, Eq. (10).

From the relation (14c), we can calculate the value of  $T_c$  if we equate  $\eta'$  with  $\eta'_{\min}=6.1$  and  $T_b$  with the experimental value of  $T_r$ ,  $\sim 500^\circ\text{C}$ . This leads to  $T_c\sim 550^\circ\text{C}$ , much lower than the value of

$\sim 680^\circ\text{C}$  obtained from the fit of the periodicity data to the theoretical results obtained from the integral-equation model. As we shall see shortly, the discrepancy can be explained qualitatively by the presence of a thermal barrier between film and substrate. The thermal barrier would not modify the form of solution of the integral equation, but only the values of the empirical parameters required to fit the results. On the other hand, the thermal barrier would make its presence felt explicitly in solving the two-dimensional heat-flow problem.

We can attempt to approximate the calculated  $F(0, V)$  in the form

$$F(0, V)\cong f/(\Gamma + V^2)^{1/2}, \quad (17b)$$

where  $f$  and  $\Gamma$  are to be determined for the best fit. Equation (17a) would then be precisely of the form Eq. (9), obtained from the integral equation, where  $\eta=f\eta'$ . The open circles in Fig. 10, representing Eq. (17b) with  $\Gamma=7.95$  and  $f=0.093$ , fit the calculated curve of  $\log[F(0, V)]^{-1}$  with  $\beta=240$  and  $M=18$  for small  $V$  and large  $V$ , but fit poorly in between. This value of  $f$  is much lower than that obtained from the integral equation fit to the periodicity data,  $f\sim 0.58$ . As we shall see, this discrepancy can also be qualitatively explained by the presence of a thermal barrier between film and substrate.

We have examined the effect of changing  $b_1$  and  $b_2$  on the values of a number of properties of  $a$ - $c$  boundary runaway. Figure 10 shows plots of  $\log[F(0, V)]^{-1}$  vs  $\log V$  for  $M=18$  and  $\beta=120$  and  $60$ , in addition to the curve for  $\beta=240$ , which corresponds to our experiment. We can interpret the reduction in  $\beta$  as due to either a decrease in  $b_2$  or an increase in  $b_1$ . The results obtained for  $V_{ac}$  and  $v_{ac}$  for  $\eta'=9.0$  (corresponding to fixed  $T_b$ , and well above  $\eta'_{\min}$  for all three values of  $\beta$ ), are listed in Table I. It can be seen that for  $b_1$  held fixed at  $0.3\ \mu\text{m}$ ,  $v_{ac}$  decreases only slightly as  $b_2$  decreases. On the other hand, for  $b_2$  held fixed at  $10^3\ \mu\text{m}$ ,  $v_{ac}$  decreases almost inversely with increasing  $b_1$ . However, in most cases it might be difficult to see this striking drop in  $v_{ac}$ , since at temperatures above  $T_r$ , spontaneous fluctuations can cause the  $a$ - $c$  transformation (see Sec. V).

Also shown in Table I are values of  $\eta'_{\min}$ , with corresponding values for  $V_{ac}$  and  $v_{ac}$ , as well as approximate values of  $f$  and  $\Gamma$ . It can be seen that  $f$  increases nearly inversely as  $\beta$  decreases, while  $\Gamma$  increases slowly. It should also be noted that  $\eta'_{\min}$  decreases as  $b_1$  increases. This means that the

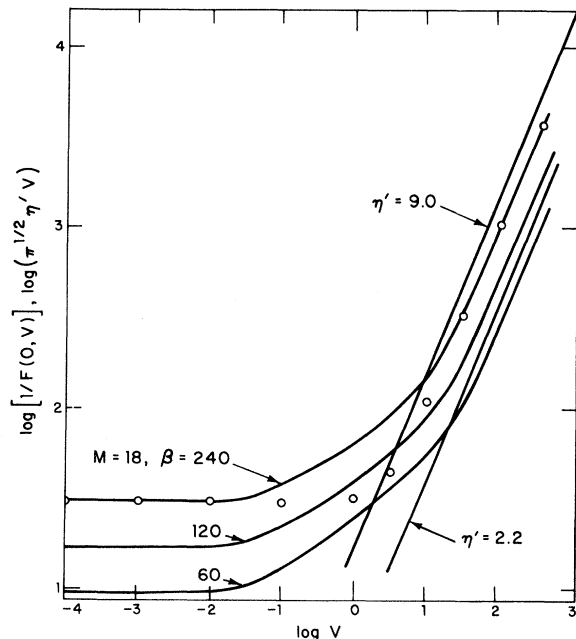


FIG. 10. Plots of  $\log[F(0, V)]^{-1}$  vs  $\log V$  for  $\beta=240$ , 120, and 60, and plots of  $\log(\pi^{1/2}\eta'V)$  vs  $\log V$  for  $\eta'=9.0$  and  $\eta'=2.2$ .

minimum value of  $T_b$  for runaway,  $T_r$ , decreases as film thickness increases. As the film thickness  $b_1$  increases, the velocity  $v_{ac}$  for  $\eta'_{\min}$  increases, but remains in the range of 100–300 cm/sec.

The small values obtained for  $T_c$  and  $f$  by applying the present theory directly to experiment can be understood if we postulate the presence of a thermal barrier between the fused-silica substrate and the amorphous Ge film in our laser-crystallization experiments.<sup>7–9</sup> The presence of a thermal barrier is not at all unreasonable, and could be readily included in the derivation of modified Eqs. (14a) and (14b). The effect of a thermal barrier is approximately equivalent to decreasing the thermal conductivity of the substrate, and is therefore qualitatively described by decreasing  $\beta$ . (Although the thermal conductivity ratio appears in  $M$ , this describes the way heat diffuses once it is transferred, and should therefore be kept fixed for this crude argument.) To obtain a rough idea of the effect of such a barrier, we examine the effect of decreasing  $\beta$  by comparing the results for  $\beta=240$  with those obtained for  $\beta=60$ . Referring to Table I, we see that for  $\beta=60$ ,  $f$  has increased to 0.331, much closer to the empirical value of 0.54 determined from the experimental data by fit-

ting the one-dimensional integral solution. Furthermore,  $\eta'_{\min}$  has dropped from 6.1 to 1.7, yielding a value of  $T_c \cong 665^\circ\text{C}$  determined from Eq. (14c). This is close to the value of  $680^\circ\text{C}$  obtained from the fit of experimental data to the integral-equation model. While this argument is very crude, it does suggest that the presence of a thermal barrier can eliminate the discrepancy between experimentally determined parameters and the results of a first-principles calculation. The presence of such a barrier would also modify the values of steady-state boundary velocity, tending to make  $V_{ac}$  less dependent on  $b_1$  and  $b_2$ .

#### IV. STEADY-STATE LASER-GUIDED SOLUTIONS

An intriguing class of steady-state solutions exists in which the  $a$ - $c$  boundary proceeds at a constant velocity on the leading edge of the scanning-laser image. Solutions of this type will be obtained for both the integral-equation model and the two-dimensional model of the  $a$ - $c$  boundary motion. The laser-guided mode of  $a$ - $c$  transformation could have important implications for the controlled growth of semiconductor films.

##### A. Integral-equation model

To find laser-guided solutions, we rewrite Eq. (3) in the frame of reference, moving at normalized velocity  $V$ , in which the laser and  $a$ - $c$  boundary temperature distributions are stationary. The result is

$$1 = T'_i(0) + \eta \int_0^{\tau_0} [V/(\tau - \tau')^{1/2}] \{ \exp[-\Gamma(\tau - \tau')] \} \{ \exp\{ -[V(\tau - \tau')]^2/(\tau - \tau') \} \} d\tau', \quad (18)$$

TABLE I. Values of a number of quantities calculated from solutions of a two-dimensional model of laser crystallization, as obtained from Fig. 10. For three values of the parameter  $\beta$ , effective parameters  $f$  and  $\Gamma$ , and  $\eta'_{\min}$  (the minimum value of  $\eta'$  for runaway) are given. With  $\eta' = \eta'_{\min}$  and  $\eta' = 9.0$ , normalized velocities  $V_{ac}$  for  $a$ - $c$  boundary runaway are obtained. For combinations of substrate ( $b_2$ ) and film ( $b_1$ ) thicknesses given, these values of  $V_{ac}$  lead to the  $a$ - $c$  boundary runaway velocities  $v_{ac}$  that are shown.

$\beta$	$f$	$\Gamma$	$\eta'_{\min}$	$V_{ac}$ ( $\eta' = \eta'_{\min}$ )	$V_{ac}$ ( $\eta' = 9.0$ )	$b_2$ ( $\mu\text{m}$ )	$b_1$ ( $\mu\text{m}$ )	$v_{ac}$ (cm/sec) ( $\eta' = \eta'_{\min}$ )	$v_{ac}$ (cm/sec) ( $\eta' = 9.0$ )
240	0.093	7.95	6.1	39	10	$10^3$	0.3	140	36
120	0.178	8.72	3.2	47	4.07	$10^3$ $5 \times 10^2$	0.6 0.3	170	14.7 29.3
60	0.331	10.15	1.7	71	1.9	$10^3$ $2.5 \times 10^2$	1.2 0.3	255	6.8 27.4

where  $T'_i(0)$  is the reduced temperature due to the scanning-laser image at the position of the  $a$ - $c$  boundary,

$$T'_i(0) = T_i(0)/(T_c - T_b).$$

As in Sec. III A, the integral in Eq. (18) can be evaluated exactly for large enough  $\tau_0$ , and we find

$$1 = T'_i(0) + \eta V \pi^{1/2} / (\Gamma + V^2)^{1/2}. \quad (19)$$

According to Eq. (19), for values of  $\eta$  and  $V$  such that  $\eta V \pi^{1/2} / (\Gamma + V^2)^{1/2} < 1$ , there is a value of  $T'_i(0)$  which will satisfy the condition for a laser-guided solution. For given values of  $V$  (determined by laser-scan velocity) and  $\eta$ , and a given reduced temperature profile due to the laser, the ( $a$ - $c$ ) boundary will ride at a distance in front of the laser image such that Eq. (19) is satisfied. It should be noted that solutions of Eq. (19) exist for arbitrarily small values of  $V$ .

### B. Two-dimensional model

It is a straightforward matter to show that the two-dimensional solution of the laser-crystallization problem also leads to laser-guided stationary solutions. The solution of the steady-state temperature distribution for the boundary-value problem in the presence of several heat sources is the superposition of the solutions in the presence of the individual heat sources.<sup>10</sup> In the presence of both a laser source of heat and the heat source due to the moving  $a$ - $c$  boundary, the exact solution for steady-state runaway, Eq. (15), becomes

$$\begin{aligned} 1 &= T'_i(0) + \eta' V \pi^{1/2} \sum_{n^+} \frac{f_{n^+}(V)}{(\Gamma_{n^+} + V^2)^{1/2}} \\ &= T'_i(0) + \eta' V \pi^{1/2} \sum_{n^-} \frac{f_{n^-}(V)}{(\Gamma_{n^-} + V^2)^{1/2}}, \end{aligned} \quad (20)$$

where  $T'_i(0)$  is the reduced temperature due to the scanning-laser image at the position of the  $a$ - $c$  boundary. The close correspondence between the exact solution Eq. (20) and the integral equation solution Eq. (19) should be noted.

Using the definition of  $F^\pm(S', V)$ , Eq. (16), we obtain for the laser-guided problem an expression analogous to Eq. (17a), which was solved to determine  $V_{ac}$  for runaway. The result is

$$\frac{\pi^{1/2} \eta' V}{1 - T'_i(0)} = [F(0, V)]^{-1}. \quad (21)$$

We may think of  $\eta' / [1 - T'_i(0)]$  as an effective value,  $\eta'_{\text{eff}}$ . Referring to Sec. III B and Fig. 10, it can then be seen that by decreasing  $1 - T'_i(0)$  the normalized laser-scan velocity  $V$  for laser-guided steady-state solutions can be reduced greatly. For a given reduced temperature distribution due to the laser scanning at velocity  $V$ , the  $a$ - $c$  boundary rides at a point in front of the laser image satisfying Eq. (21).

Both the integral-equation solution and the two-dimensional solution yield steady-state laser-guided modes of motion of the  $a$ - $c$  boundary, at velocities lower than those for unguided runaway. However, attempts to find such solutions by numerical integration of Eq. (3) have thus far failed. The difficulty may be associated with the singular initial-velocity characteristic of Eq. (3). Elimination of this unphysical initial singularity could lead to solutions yielding stable laser-guided motion (see discussion in Sec. V).

### V. DISCUSSION

One of the important assumptions made in calculating the motion of the  $a$ - $c$  boundary for both the one-dimensional integral equation and two-dimensional solution was the existence of a sharply defined transition temperature  $T_c$ . In fact, the velocity of growth of crystalline material directly from the amorphous state  $\dot{S}(T)$  is a function of temperature, increasing rapidly as the temperature is raised. This could be interpreted as determining the temperature  $T_c(\dot{S})$  at which the transition can take place at a value of  $\dot{S}$  demanded by the heat-flow calculation. From this simplistic point of view, over a wide range of values of  $\dot{S}$ ,  $T_c$  varies relatively little and can be taken as constant. As already pointed out in Sec. II B, the model solution of the integral equation at the beginning of each period of boundary motion requires infinite velocity, and the presence of amorphous and fine-grained material in the initial portion of each period may be related to the limits on the rate at which crystalline growth can occur.

We could attempt to improve the approximate description of the boundary motion using the integral Eq. (3) by replacing  $\eta$  by the quantity

$$\eta_{\text{eff}}(\dot{S}) = fL(\dot{S}) / [T_c(\dot{S}) - T_b], \quad (22)$$

where  $T_c(\dot{S})$  is the critical temperature appropriate to the value of  $\dot{S}$ , and  $L(\dot{S})$  is an effective latent heat which is that portion emitted when partial

conversion to crystalline material takes place at boundary velocity  $S$ . We now interpret  $S$  as the velocity of a "heat-flow boundary," which is identical to the  $a$ - $c$  boundary when that boundary is well defined. We can see that at large  $S$ ,  $\eta_{\text{eff}}(S)$  is reduced because  $L(S)$  is reduced and  $T_c(S)$  is increased. At lower values of  $S$ ,  $L(S) \rightarrow L$ , and  $T_c(S) \sim T_c$ . The introduction of an  $\eta_{\text{eff}}(S)$  of this form could eliminate the unphysical singularity in the initial motion present in Eq. (3), while still yielding a very high initial value of  $S$ , consistent with the initial amorphous and fine-grained polycrystalline material in each period. The introduction of an  $\eta'_{\text{eff}}(V_{ac})$  in Eq. (17a) would also modify the exact solutions obtained for  $V_{ac}$  from the two-dimensional boundary-value problem.

As mentioned in Sec. II B, the value of  $T_c$  obtained by fitting the results of the integral-equation solution to our experimental data was  $T_c \approx 680^\circ\text{C}$ , very close to the value of  $696^\circ\text{C}$  predicted by Bagley and Chen<sup>11</sup> for the transition temperature from the amorphous to liquid state of Ge. It has been suggested<sup>15,16</sup> that "explosive" crystallization (or runaway) may correspond to the occurrence of this transition, and some experimental evidence supporting this point of view has been obtained.<sup>17</sup> If, in fact,  $T_c$  does correspond to the amorphous-to-liquid transition, the assumption of a fixed  $T_c$  over a range of  $S$  is reasonable. Once the transition from amorphous to liquid state had occurred, the unstable liquid would rapidly transform to the crystalline state.<sup>11</sup> For small temperature differences across a thin liquid layer, the treatment we have presented would require no major modification.

Throughout this paper, we have treated the amorphous and crystalline regions of the semiconductor film undergoing laser crystallization as isotropic and homogeneous regions, with the transformation from the amorphous to the crystalline state governed by macroscopic heat-flow equations. An important ingredient absent from this description, and essential for even a qualitative understanding of crystallized-film morphology, is the role of nucleation centers<sup>18</sup> and "nucleation events." Because the exact nature of the  $a$ - $c$  transformation in laser crystallization is not yet certain, we will not attempt a detailed description of nucleation. We regard a nucleation event as a spontaneous, localized fluctuation which initiates a transformation from the amorphous to the crystalline state and produces a small increase in local temperature above the background determined by macroscopic heat flow. A nucleation event has a probability of oc-

currence which increases with the density of nucleation centers (which depends on film perfection) and with increasing temperature. For  $T_b$  just below  $T_r$  (the lowest temperature for runaway), nucleation events can produce transformation from the amorphous to crystalline state in small regions of finite range about nucleation centers.<sup>19</sup> For  $T_b \sim T_r$ , and in the absence of an external disturbance such as a laser beam, multiple nucleation events can occur, overlapping and spontaneously transforming the entire film to the crystalline state in a short time if the probability of such events is high enough. From the discussion of Sec. III B, the minimum value of  $T_b$  for runaway  $T_r$  is higher for thinner films, decreasing as the films become thicker. Since the probability of nucleation events increases with increasing temperature, spontaneous transformation to the crystalline state should occur most readily at  $T_b \sim T_r$  for thin amorphous films. This is consistent with our observation of laser-induced runaway for films of thickness greater than  $1 \mu\text{m}$ , while only spontaneous transformation is observed for films  $0.3\text{-}\mu\text{m}$  thick.

The occurrence of nucleation events appears to play a major role in the morphology of laser-crystallized films. In the films that we have examined in detail, the elongated crystallites within each periodic feature form a roughly chevronlike pattern, with the two halves of the pattern symmetrical about an axis that is parallel to the laser-scan direction and located near the center of the laser image. The elongated crystallites on each side of the pattern have their long axes aligned along [100] directions. A blown-up picture of a crystallized film near the center axis of the chevron pattern is shown in Fig. 11. The "origin" of the chevron pattern within each periodic feature is a small region located somewhere near the center axis. The exact lateral position of the origin varies from one period to the next over a distance of perhaps  $100 \mu\text{m}$  ( $\sim 10\%$  of the slit-image length). This suggests that the origin represents the position of the first nucleation event within a periodic feature where the heat-flow boundary is moving slowly enough for large crystallites to form. The first nucleation event would be likely to occur near the center axis, since the laser-slit image is an ellipse of high-aspect ratio and the temperature should therefore first reach  $T_c$  near this axis. Once nucleation and growth of large crystallites began, heat would flow forward, but also laterally, raising the temperature and inciting the nucleation of new growth centers laterally. The direction of growth

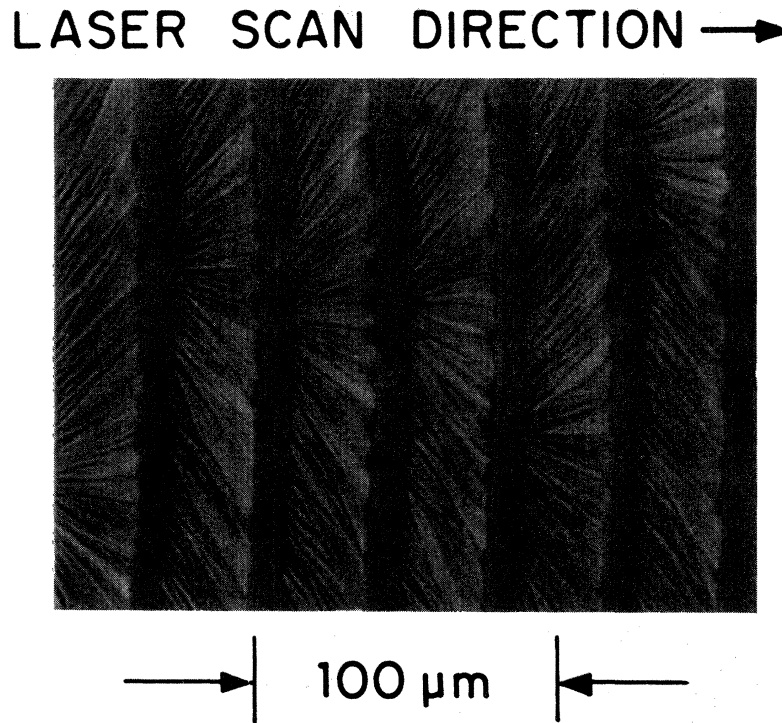


FIG. 11. Blown-up view of periodic features in a Ge film crystallized by the slit image of a laser. Picture taken near the center axis of the slit image shows the origins of chevron pattern.

from these centers would tend to be channeled by such factors as interaction with neighboring crystallites already formed,<sup>20</sup> strong anisotropy in the directional dependence of growth rate, and perhaps stresses in the film. The result of all of these influences would combine in a statistical way, but it can be argued that the outcome would be largely determined by the tendency of growth to occur along the direction of the temperature gradient at the *a-c* boundary, combined with the high rate of growth along a [100] direction compared to other crystallographic directions. Motion of the *a-c* boundary would occur laterally as well as along the laser-scan direction, but a periodic morphological pattern would still result. This description is consistent with the observed chevron pattern, and could serve as the basis for a more complete analysis.

In Sec. IV we discussed a class of laser-guided stationary solutions of both the integral equation formulation and the two-dimensional formulation of *a-c* boundary motion. The problem remains of identifying spatial and temporal initial conditions which allow the boundary motion to settle into such a constant-velocity stationary state. The solution of this problem could have important implications for the possibility of producing uniformly

aligned, laser-crystallized semiconductor films. In studying solutions of the integral Eq. (3), we found that for, say,  $\eta=0.6$  and a given value of  $V$ , no matter how large,  $S(\tau)$  would always exhibit periodic motion of the type shown in Fig. 2 when a small enough value of  $\delta t$  was used in numerical integration (see Sec. II A). We believe this behavior of the solutions is due to the unphysical singularity in the initial velocity given by Eq. (3), so that the *a-c* boundary is always predicted to outrun the laser and stop for  $T_b < T_r$ . As we have suggested, this singular behavior might be eliminated from the mathematical description by replacing  $\eta$  in Eq. (3) by a velocity dependent  $\eta_{\text{eff}}$  given by Eq. (22). This would imply that the initial motion of the *a-c* boundary is characterized by some finite velocity  $V_0$ . For laser-scan velocity  $V > V_0$ , we would then expect a damped oscillatory behavior of  $S(\tau)$ , with the motion settling into a laser-guided stationary state. A slow decrease in  $V$  could perhaps then lead the *a-c* boundary motion into a laser-guided stationary state at a lower velocity, with the *a-c* boundary riding close to the thermal image of the scanning laser. However, the stability of such motion remains questionable. All of these points are highly speculative, and require further exploration.

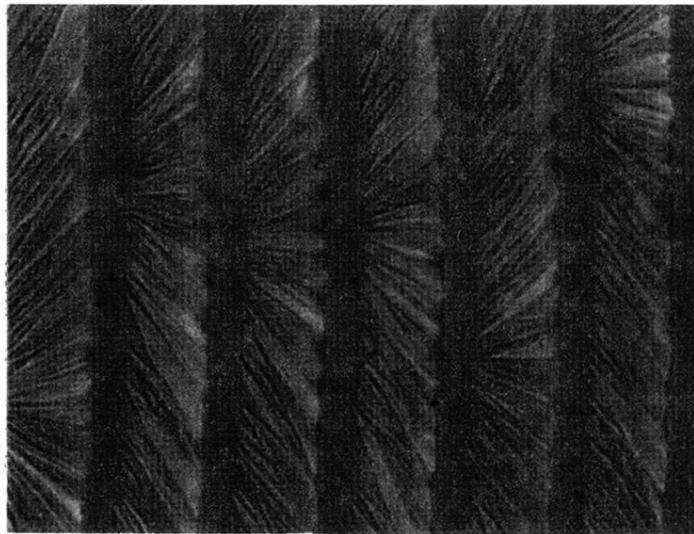
## ACKNOWLEDGMENTS

We are grateful to A. J. Strauss for his interest, advice, and encouragement during the entire course

of this research. This work was supported by the Department of the Air Force, the Department of Energy, and the Solar Energy Research Institute.

- 
- <sup>1</sup>N. A. Blum and C. Feldman, *J. Non-Cryst. Solids* **22**, 29 (1976).
- <sup>2</sup>N. A. Blum and C. Feldman, *J. Non-Cryst. Solids* **11**, 242 (1972).
- <sup>3</sup>H. S. Chen and D. Turnbull, *J. Appl. Phys.* **40**, 4214 (1969).
- <sup>4</sup>J. C. C. Fan and C. H. Anderson, *J. Appl. Phys.* **52**, 4003 (1981).
- <sup>5</sup>See, for example, T. Takamori, R. Messier, and R. Roy, *Appl. Phys. Lett.* **20**, 201 (1972); K. J. Callanan, A. Matsuda, A. Mineo, T. Kurosu, and M. Kikuchi, *Solid State Commun.* **15**, 119 (1974); C. E. Wickersham, G. Bajor, and J. E. Greene, *ibid.* **27**, 17 (1978); R. A. Lemons and M. A. Bosch, *Appl. Phys. Lett.* **39**, 343 (1981); F. M. Aymerich and A. Delunas, *Phys. Status Solidi A* **31**, 165 (1975).
- <sup>6</sup>T. Takamor, R. Messier, and R. Roy, *J. Mater. Sci.* **8**, 1809 (1973); A. Mineo, A. Matsuda, T. Kurosu, and M. Kikuchi, *Solid State Commun.* **13**, 329 (1973).
- <sup>7</sup>J. C. C. Fan, H. J. Zeiger, R. P. Gale, and R. L. Chapman, *Appl. Phys. Lett.* **36**, 158 (1980).
- <sup>8</sup>H. J. Zeiger, J. C. C. Fan, B. J. Palm, R. P. Gale, and R. L. Chapman, in *Proceedings of Symposium on Laser and Electron Beam Processing of Materials*, edited by C. W. White and P. S. Percy (Academic, New York, 1980), p. 234.
- <sup>9</sup>R. L. Chapman, J. C. C. Fan, H. J. Zeiger, and R. P. Gale, *Appl. Phys. Lett.* **37**, 292 (1980).
- <sup>10</sup>H. J. Zeiger, J. C. C. Fan, B. J. Palm, R. L. Chapman, and R. P. Gale, Technical Report No. 558, Lincoln Laboratory, MIT (unpublished).
- <sup>11</sup>B. G. Bagley and H. S. Chen, in *Laser-Solid Interactions and Laser Processing* (Materials Research Society, Boston, 1978), edited by S. D. Ferris, H. J. Leamy, and J. M. Poate (AIP, New York, 1978), p. 97.
- <sup>12</sup>H. S. Carslaw and J. C. Jaeger, *Conduction of Heat in Solids* (Oxford University Press, London, 1959), p. 293.
- <sup>13</sup>M. W. Geis, D. C. Flanders, and H. I. Smith, *Appl. Phys. Lett.* **35**, 71 (1979).
- <sup>14</sup>P. Nath and K. L. Chopra, *Phys. Rev. B* **10**, 3412 (1974).
- <sup>15</sup>R. B. Gold, J. F. Gibbons, T. J. Magee, J. Peng, R. Ormond, V. R. Deline, and C. A. Evans, Jr., in Ref. 8, p. 221.
- <sup>16</sup>G. H. Gilmer and H. J. Leamy, in Ref. 8, p. 227.
- <sup>17</sup>H. J. Leamy, W. L. Brown, G. K. Celler, G. Foti, G. H. Gilmer, and J. C. C. Fan, *Appl. Phys. Lett.* **38**, 137 (1981).
- <sup>18</sup>See, for example, B. Chalmers, *Principles of Solidification* (Wiley, New York, 1964).
- <sup>19</sup>M. Larsen, H. J. Zeiger, and B. J. Palm, *Appl. Phys. Commun.* **1**, 69 (1981).
- <sup>20</sup>R. P. Gale, J. C. C. Fan, R. L. Chapman, and H. J. Zeiger, in *Proceedings of the Materials Research Society Symposium on Defects in Semiconductors*, edited by J. Narayan and T. Y. Tan (Elsevier, New York, 1981), p. 439.

LASER SCAN DIRECTION →



→ | 100  $\mu\text{m}$  | ←

FIG. 11. Blown-up view of periodic features in a Ge film crystallized by the slit image of a laser. Picture taken near the center axis of the slit image shows the origins of chevron pattern.

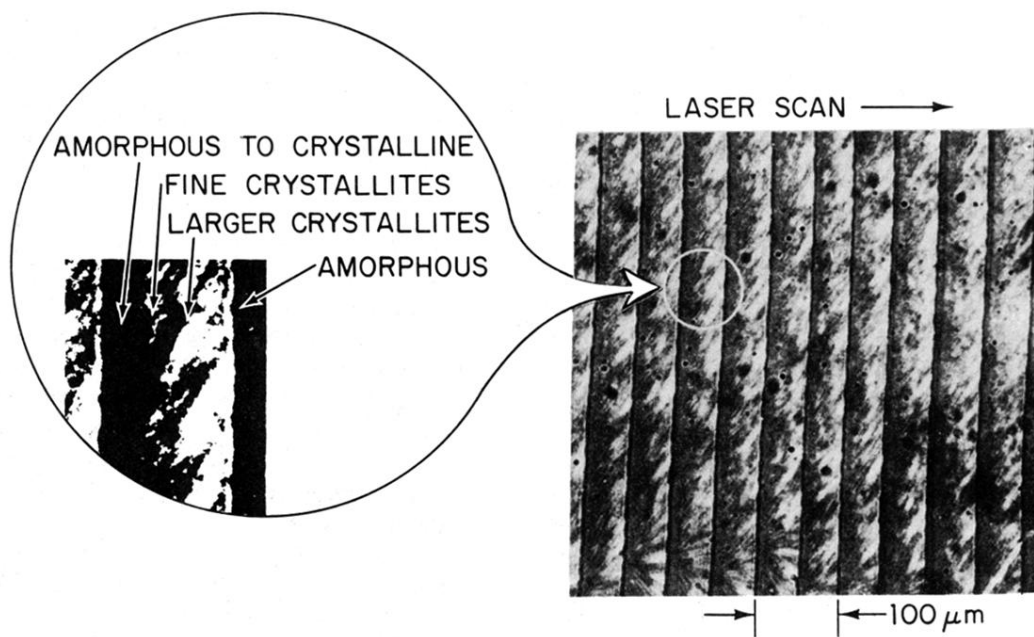


FIG. 3. Optical transmission micrograph of a laser-crystallized Ge film showing periodic structural features. Inset is expanded view illustrating four different microstructure regions.

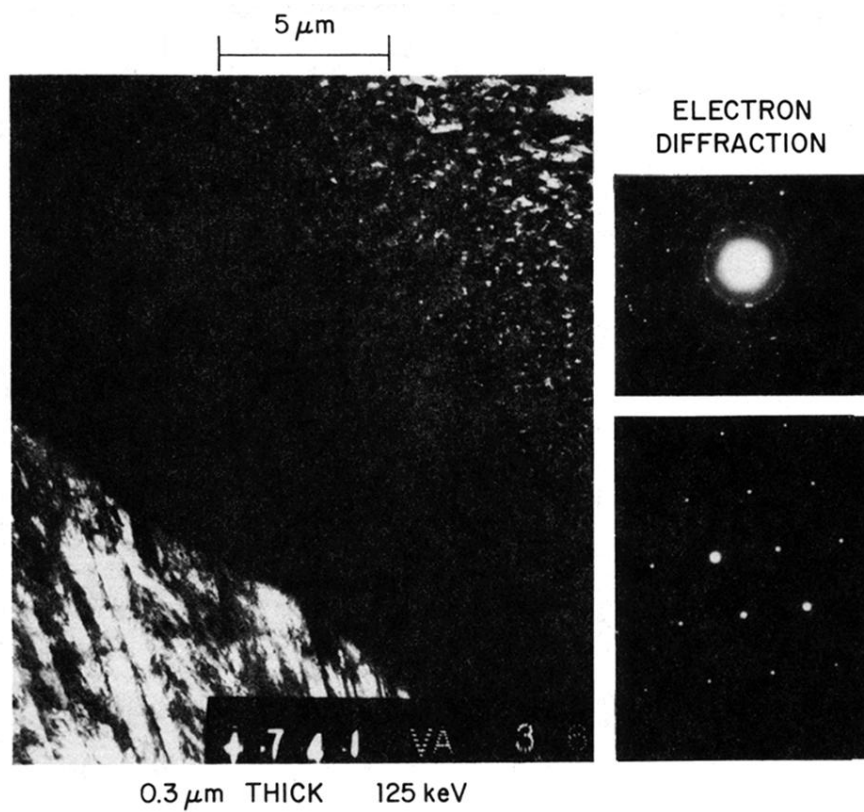


FIG. 4. Left: Bright-field transmission-electron micrograph of a laser-crystallized Ge film, illustrating four different microstructure regions. Right: Transmission-electron diffraction patterns for fine-grained and large-grained regions (upper and lower, respectively).